Boundary-Layer Meteorol (2014) 150:449–467
DOI 10.1007/s10546-013-9880-4

ARTICLE

Observing Entrainment Processes Using a Small Unmanned Aerial Vehicle: A Feasibility Study

Sabrina Martin · Frank Beyrich · Jens Bange

Received: 16 December 2012 / Accepted: 23 October 2013 / Published online: 3 December 2013

Abstract Measurement flights with the meteorological mini aerial vehicle (M^2AV) were performed in spring 2011 to assess the capability of an unmanned aerial vehicle (UAV) to measure the structure of the transition zone between the convective boundary layer and the stably stratified free atmosphere. The campaign took place at the Meteorological Observatory Lindenberg/Richard-Aßmann-Observatory of the German Meteorological Service. Besides the M^2AV flights, observations were made from a 12-m and a 99-m tower, a sodar, two ceilometers, radiosondes, and a tethered balloon with sensor packages at six different levels. M^2AV measurements were intentionally combined with remote sensing systems. The height range of the entrainment zone as well as its diurnal cycle were provided by the remote sensing instruments. The UAV provided the high-resolution in situ data of temperature and wind for the study of turbulent processes. It is shown that the M^2AV is able to maintain constant altitude with very small deviations—a pre-requisite to study processes inside the often quite thin entrainment zone and that M^2AV high-resolution wind and temperature measurements allow for very detailed studies of the fine structure of the atmosphere and thus for the identification of quite local and/or short-duration processes such as overshooting thermals or downward intrusions of warm air. Spatial series measured by the M^2AV during horizontal flights show turbulent exchange of heat in short turbulent bursts at heights close to and within the entrainment zone. Scaled vertical profiles of vertical velocity, potential temperature variance, and sensible heat flux confirm the general shape found by previous measurements and numerical studies.

S. Martin (✉)
Institut für Geoökologie, Technische Universität Carolo-Wilhelmina Braunschweig, Langer Kamp 19c, 38106 Braunschweig, Germany
e-mail: sabrina.martin@tu-braunschweig.de

F. Beyrich
Meteorological Observatory Lindenberg – Richard-Aßmann-Observatory, German Meteorological Service, Am Observatorium 12, 15848 Tauche OT Lindenberg, Germany

J. Bange
Centre for Applied Geoscience, Eberhard Karls Universität Tübingen, Hölderlinstr. 12, 72074 Tübingen, Germany

Keywords Entrainment · Inversion layer · Turbulence · Unmanned aerial vehicle

1 Introduction

During daytime over land, radiative heating of the surface drives intense thermal turbulence in the atmospheric boundary layer (ABL). This leads to the formation of a convectively driven mixed layer that is usually separated from the stably stratified free atmosphere by a temperature inversion (Stull 1988). This capping inversion restrains the domain of intense surface-generated turbulence and acts as a lid to the vertical exchange (mixing) of trace constituents as water vapour and pollutants (Stull 2000). The most energetic convective updrafts might be able to penetrate into this capping inversion, thereby initiating the downward transport of warmer, drier, and less polluted air from the free atmosphere into the ABL; this process is termed entrainment. Entrainment thus is a local phenomenon of discrete events that finally supports ABL growth (e.g., Bange et al. 2007).

The height range over which entrainment takes place is called the entrainment zone, and can be defined based on the profile of the turbulent heat flux (Stull 1988). Definitions based on turbulence statistics are quite common as well, since the instantaneous interface between the convective mixed layer and the free atmosphere above may be very thin (e.g., Träumner et al. 2011). These definitions either use mixing ratios between boundary-layer and free-atmosphere air or frequency distributions of instantaneous boundary-layer heights. The experimental analyses regarding entrainment processes performed by Deardorff et al. (1980) included simulations of the atmospheric mixed layer and the entrainment zone in laboratory experiments. Besides other results it was found that the thickness of the entrainment zone, relative to the depth of the mixed layer, is in the range between 0.2 and 0.4. Other key quantities regarding the entrainment zone are the entrainment velocity and the entrainment fluxes of heat, moisture, and chemical species (Angevine et al. 1998; Träumner et al. 2011).

The height of the convective boundary layer (CBL) can be identified from profile measurements using in situ systems such as radiosondes, tethered balloons and aircraft (e.g., Angevine et al. 1994; Nilsson et al. 2001; Siebert et al. 2003), and of remote sensing systems such as sodar, wind profiler, and lidar (e.g., Beyrich 1997; Cohn and Angevine 2000; Emeis et al. 2004; Träumner et al. 2011). CBL height (z_i) estimates from sodar and wind profilers are typically based on the backscattered signal of the instrument that is proportional to the values of the refractive index structure parameter. For acoustic and electromagnetic waves this parameter has a local maximum at the CBL height due to turbulence and the strong gradients of temperature and humidity across the entrainment zone (e.g., Beyrich and Görsdorf 1995). Lidar signals originate from aerosol backscatter for many instruments, and the CBL height estimates from these systems are often based on the strongest gradient of backscattered laser radiation. The aerosol content is enhanced within the turbulent mixed layer, and it is normally much lower in the free troposphere above, which leads to a large backscatter gradient at the CBL top (Emeis et al. 2004).

Measurements of the boundary-layer growth, visualization of entrainment processes and characterization of the turbulence throughout the ABL is possible using Doppler lidar (Träumner et al. 2011). The entrainment velocity as well as the temperature and humidity across the inversion layer can be measured and the entrainment flux can be estimated by manned aircraft (Lenschow et al. 1999; Bange et al. 2007; Canut et al. 2010).

The above mentioned techniques do not allow for high temporal and spatial resolution in-situ measurements within the entrainment zone. The aim of this article is to determine whether unmanned aerial vehicles (UAV) might be able to fill that observational gap. UAV

are innovative measurement systems. Compared to manned aircraft UAV allow operations at lower airspeeds resulting in a higher spatial resolution, the costs for operation are less as is the organizational effort. Their small size and their capability to operate at a prescribed height level with very small variation only make them ideal candidates to fly within the relatively thin entrainment zone. Equipped with sensors allowing for fast-response wind and temperature measurements (and hence for high temporal and spatial resolution) UAV are supposed to allow detailed studies of entrainment processes. While the ability of identifying the CBL height from UAV data was already demonstrated in, e.g., Reuder et al. (2009), Martin et al. (2011) and Dias et al. (2012), this study presents, to the knowledge of the authors, the first attempt to analyze the structure and processes in the transition zone between a convectively mixed layer and a stably stratified atmosphere aloft using in situ UAV data.

2 Experiment

A short measurement campaign was performed on March 2–3, 2011, at the Meteorological Observatory Lindenberg/Richard-Aßmann-Observatory (MOL-RAO) of the German Meteorological Service (DWD). The observatory is located about 65 km south-east of Berlin and has a long tradition in measuring the vertical structure of the atmosphere, dating back to 1905 (Berger and Hantel 2005). A comprehensive and continuous boundary-layer measurement program has been performed since 1998, with a special boundary-layer field site (the so-called GM Falkenberg) as a central experimental facility (Beyrich et al. 2006). The observatory operates a large number of meteorological measurement systems including remote sensing systems and in-situ soundings (Neisser et al. 2002; Beyrich and Engelbart 2008). For the present study data from radiosondes, sodar, ceilometer, towers (12 and 99 m height) and a tethered balloon system were analyzed. All of these measurement systems are routinely operated by the DWD, and only the tethered balloon was especially operated for the present study.

The heterogeneous terrain in the area around the MOL-RAO is dominated by agricultural farmland. During the 2-day campaign the weather situation in Germany was influenced by a high pressure system located over Denmark and a low pressure system located over Sardinia. At the time of the experiment, eastern Germany was dominated by easterly low-level flow. The air temperature decreased to $-4\,^{\circ}\mathrm{C}$ at night and reached up to 6 °C during the day. The sky was almost cloudless with only temporary alto-cumulus clouds ($<1/8$ cloud cover). Due to the early season, CBL growth was expected to be relatively low with a maximum z_i below 1,000 m. We explicitly waited for such a situation with an undisturbed development of the CBL, a maximum z_i that can safely be reached by the UAV, and low mixed-layer growth rates such that stationarity can be assumed over short time periods. All together this represents an ideal case for a field campaign aiming at the analysis of entrainment processes using small UAV.

Figure 1 presents the locations of the systems during the campaign. The two towers, the sodar and the tethered balloon were operated at the GM Falkenberg whereas the radiosondes were launched about 5 km northwards at the observatory site in Lindenberg. The flight paths of the meteorological mini aerial vehicle (M^2AV, blue line) mainly consisted of flight legs directed southward or northward with a range of about 3 km. Flight legs at constant altitude as well as slant flights with continuously increasing or decreasing altitude were performed.

Figure 2 illustrates an overview of the relevant M^2AV flights during the campaign. On March 2, four vertical profiles were performed with a maximum altitude of about 500 m a.g.l. The CBL height was expected to be below the maximum altitude of the profiles, and the aim was to gain a detailed image of the vertical structure of the ABL. Besides, the quality of

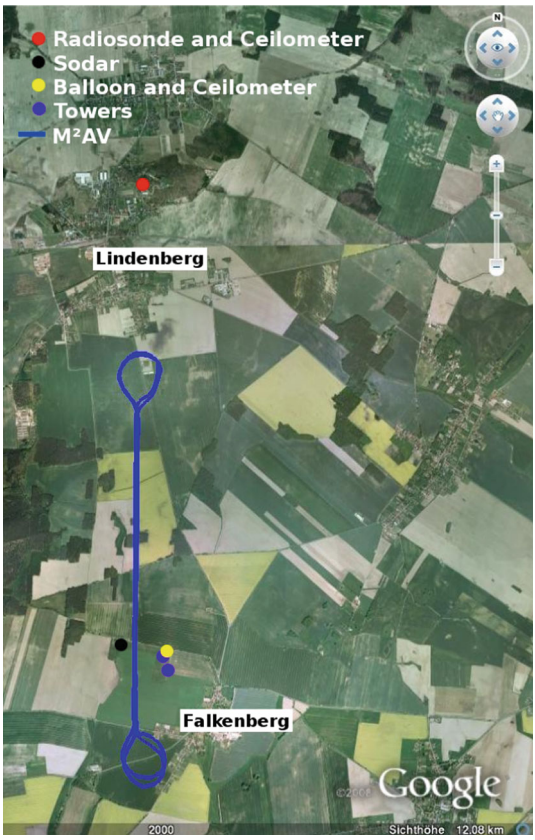

Fig. 1 Location of the instruments that were used for the analysis. The *red dot* represents the location of one ceilometer and the radiosonde ascents at Lindenberg. The sodar (*black dot*), the towers (*purple dot*), the second ceilometer and the balloon system (*yellow dot*) were operated about 5 km south of the radiosonde ascents, close to Falkenberg. The flight path of the M^2AV is marked with a *blue line* going from Falkenberg towards Lindenberg with a leg length of about 3 km (*Source* DWD boundary-layer field site. 52.1877°N and 14.0734°E. Google Earth. January 1 2008; March 9 2012)

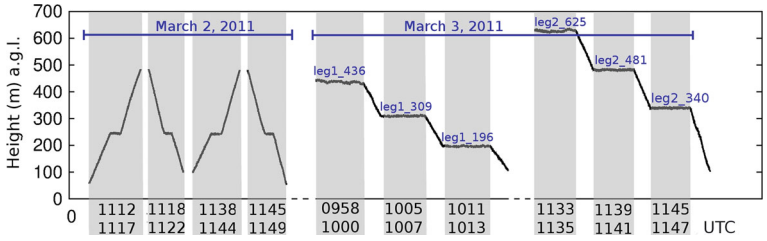

Fig. 2 Overview of the M^2AV flight legs and slant flights during the campaign in March 2011. The specific sections of each flight used for the analysis are highlighted using *grey boxes* and the corresponding time periods are provided on the *x*-axis of the diagram

the M^2AV identification of the inversion base was studied. On March 3, two flights were performed to analyze the structure of the entrainment zone in comparison with the structure of the underlying CBL. The horizontal flight legs at various altitudes were performed along the same track.

2.1 Measurement Systems

This analysis mainly focuses on the measurements from the automatically operating research UAV M^2AV. The M^2AV is a twin-engine Mini-UAV, constructed by the Institute of Aerospace

Systems (ILR) of the Technische Universität Braunschweig (Spieß et al. 2007). The M^2AV has a wingspan of 2 m and a maximum take-off weight of approximately 6 kg including 1.5 kg of meteorological payload. The cruising speed of about 22 m s^{-1} and the electrical power supply for about 50–60 min of flight allow flight distances of up to 70 km. Heights up to 1,500 m above the ground can be reached by the M^2AV still ensuring visual contact to the ground staff, as presented in Martin et al. (2011). Technically, maximum elevation above sea level up to 4,000 m is possible. The M^2AV is automatically operated by an electronic autopilot developed at the ILR (Buschmann et al. 2004). Automatic operations allow measurement flights in the lower ABL over larger distances outside the range of sight and in remote areas if permitted by the civil aviation authority (CAA). During the present campaign flights outside the range of sight and flights above populated areas were not permitted by the CAA. Flight legs longer than ± 1 km from the take-off/landing area were realized by positioning human pilots at the ground close to the northern and southern turning points of the flight track such that there was always a pilot within 1 km from the aircraft's actual position. This way of operation ensured visual contact with the UAV and the possibility of interacting at any time of the operation. A NOTAM (notice to airmen) was published to minimize interference with conventional air traffic, but in case of interference the human safety pilots had to react by changing the flight track or flight altitude of the M^2AV.

In automatic flight mode the M^2AV follows the flight pattern that was sent to the aircraft before take-off (van den Kroonenberg et al. 2008). Within the telemetry range of 5 km the ground staff is able to follow and monitor the position, attitude and speed of the aircraft. Changes of the way-points and altitudes are possible within that range through radio communication. The UAV is launched and landed by a human pilot, but operates automatically when following the flight mission.

Operation limitations of the M^2AV are due to wind speeds at the flight altitude, which need to stay below 10 m s^{-1} for safe operation. It is possible to operate the M^2AV at night and within clouds. For both cases, permission of the local civil aviation authorities (CAA) is required. The latter case is currently not allowed at all, whereas flights at night were performed several times with the M^2AV during past campaigns. Since the M^2AV is not yet rainproof concerning the measurement electronics, operation in precipitation is currently not possible.

The M^2AV and its instrumentation are presented in Fig. 3. Since the main application of the M^2AV is the investigation of turbulent structures and fluxes in the ABL, the aircraft is

Fig. 3 The M^2AV flying past the meteorological tower at MOL-RAO and its sensor dome

equipped with fast sensors and data acquisition at 100 Hz (van den Kroonenberg et al. 2011). The meteorological sensor dome includes a 5-hole probe and pressure sensors for measuring the three-dimensional wind vector with respect to the Earth, atmospheric pressure and altitude. The calculation of the wind vector is described in detail in van den Kroonenberg et al. (2008), where it was found that the UAV is capable of measuring the mean and the turbulent wind vector with 40-Hz temporal resolution. A Vaisala HMP 50 is used for temperature and humidity measurements, and a thermocouple for measuring fast temperature fluctuations (Martin et al. 2011). By complementary filtering, the signals of the two temperature sensors are combined, resulting in long-term stability with high accuracy and 10-Hz temporal resolution in an ambient-temperature range from −40 to +60 °C (van den Kroonenberg et al. 2011; Martin et al. 2011). The sensor dome is mounted at the nose of the M^2AV to minimize the aircraft's influence on the measurements and to ensure the sensors are positioned close to each other. Also part of the meteorological payload is an inertial measurement unit and a three-dimensional global positioning system (GPS) measuring and storing precise information about time, aircraft position, attitude and speed (van den Kroonenberg et al. 2008). Real-time monitoring of meteorological M^2AV data was not provided by the system during the campaign.

Several UAV presented in the literature are able to measure mean meteorological quantities, such as the Aerosonde (Holland et al. 2001; Curry et al. 2004) and the small unmanned meteorological observer (SUMO, Reuder et al. 2009; Mayer et al. 2010) or they provide data with temporal resolutions up to 1 Hz, such as the Aerolemma-3 (Dias et al. 2012). To our knowledge, the M^2AV is currently the only UAV in its class of relatively small aircraft with a payload less than 1 kg that is able to measure the turbulent fluctuations of the three-dimensional wind vector and the air temperature with temporal resolutions of 10 Hz and higher, as presented in van den Kroonenberg et al. (2008), van den Kroonenberg et al. (2011) and Martin et al. (2011).

Results of the vertical kinematic sensible heat flux $\overline{w'\theta'}$ measured by the M^2AV are presented in Sect. 3 as well as the vertical velocity variance σ_w^2, and the potential temperature variance σ_θ^2 calculated from M^2AV measurements. For the calculation of these (co-)variances, the entire flight leg was used. Although the flights were performed above heterogeneous terrain (see Fig. 1), the surface patches were small, and no particular surface type was dominant since the agricultural vegetation was not active in that early season of the year. In such a situation the simple rule 'the longer, the better' applies in order to reduce the statistical error (Lenschow and Stankov 1986; Lenschow et al. 1994; Mann and Lenschow 1994; Bange 2009).

Surface flux values, which were necessary to calculate scaled vertical profiles of $\overline{w'\theta'}$, σ_w^2, and σ_θ^2, were measured by a large aperture scintillometer (LAS) and by an eddy-covariance measurement system at the field site close to Falkenberg. Both systems were operated by the DWD. The analyzed M^2AV flights were performed along the scintillometer path to ensure compatibility between measurement data of the two systems. The scintillometer path is about 2 km longer than the performed M^2AV flight legs. The distance of 5 km between transmitter and receiver of the LAS ensures representativeness at a regional scale. The measurements of the eddy-covariance system are considered as representative for the surface below the flight path as well since easterly winds dominated during the campaign for which agricultural farmland is the dominant land use in the incoming flow sector, and the vegetation was still dormant at the beginning of March.

Measurements of the two towers of 12-m and 99-m height are used for comparison with data of the M^2AV. The towers carry standard meteorological sensors at different heights with a more dense coverage close to the surface. For this analysis temperature measurements

averaged over 10 min were used. The UAV was intentionally combined with remote sensing systems. On the one hand the UAV alone did not allow determination of the height range of the entrainment zone since it allows for instantaneous profile measurements only. On the other hand the UAV delivered much information that the accompanying remote sensing instruments were not able to provide, namely the high-resolution in situ data of temperature and wind for studying turbulent processes. So, the CBL heights were derived from sodar (DSDPA.90-64, METEK, Germany) and ceilometer (CHM 15k, Jenoptik, Germany) measurements. For both instruments high time-resolution (20 and 15 s, respectively) profiles of backscatter intensity were analyzed for the occurrence of elevated maxima (sodar) or significant gradients (ceilometer). This analysis was done by semi-automatic algorithms interactively applied by a human expert prescribing the height range to analyze the shape of a reference pattern, possible smoothing of the profiles and signal-to-noise ratio threshold values (e.g., Beyrich and Gryning 1998, for the sodar case). In situ profile measurements of Vaisala RS92 radiosondes were also used for comparison with M^2AV data regarding the structure of the ABL. A Vaisala DigiCORA tethered balloon system equipped with six sondes at different, varying heights along the tether line was also used to support the aircraft data (Neisser et al. 2002; Beyrich and Engelbart 2008).

2.2 Convective Boundary-Layer Height Evolution

The analysis presented herein is based on a two-day measurement campaign performed in March 2011. In Fig. 4, the CBL heights estimated from the sodar and ceilometer (MCO) data as well as the measurement periods of the different episodically operating systems are presented. On both days, the sodar and MCOs observed a slow but steady mixed-layer growth until about 1030 UTC. After a decrease of z_i, more rapid growth and larger variability was measured. CBL heights below ≈300 m could not reliably be deduced from the MCO data due to incomplete overlap between the transmitting and receiving telescopes of the instruments. Estimation of z_i from the sodar data was not possible in the afternoon during the campaign, when z_i exceeded the sodar range of about 600 m.

The coloured boxes in the diagrams indicate the time periods of the operation of the non-continuously operated measurement systems without presenting any measurement results.

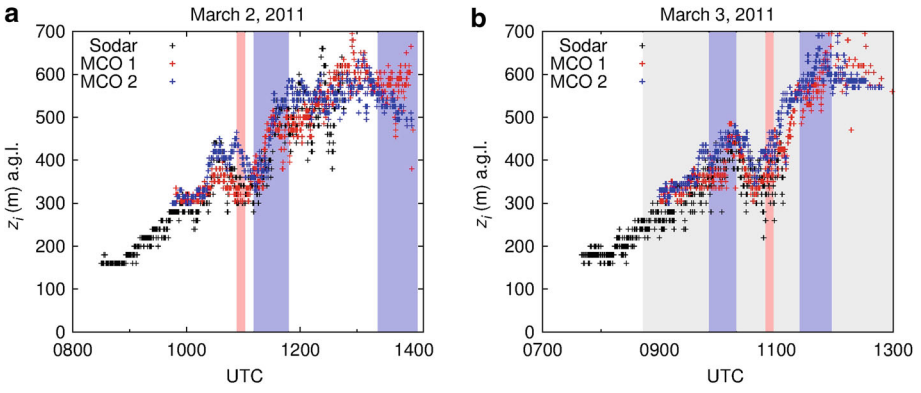

Fig. 4 The CBL height determined from the sodar (*black crosses*), the ceilometer in Lindenberg (MCO 1, *red crosses*), the ceilometer in Falkenberg (MCO 2, *blue crosses*) and the measurement periods of the different systems. *Light blue boxes* represent the time periods of the M^2AV flights, *light red lines* indicate the time of the radiosonde ascents, and the *grey box* marks the time period of the tethered balloon measurement

Table 1 Flight altitudes (z) with standard deviations (σ_z) and leg length for all flight legs performed on March 3 2011 by the M^2AV

Flight number	Leg name	UTC (hhmm)	z (m)	σ_z (m)	Length (m)	z_i (m)	z/z_i
1	leg1_436	0958–1000	436	2.8	3,235	410	1.07
1	leg1_309	1005–1007	309	0.6	3,179	410	0.75
1	leg1_196	1011–1013	196	1.3	3,330	410	0.48
2	leg2_625	1133–1135	625	1.3	2,474	606	1.02
2	leg2_481	1139–1141	481	1.0	2,868	606	0.79
2	leg2_340	1145–1147	340	1.0	3,323	606	0.56

Also presented are averaged CBL heights estimated from data of one sodar and two ceilometers during the time of flight and averaged over the three systems. The ratio of flight altitude to z_i is given in the last column

The M^2AV flights, marked with light blue boxes, were performed around noon and 1400 UTC on March 2, 2011 and around 1000 UTC and noon on March 3, 2011. The second flight of the first measurement day was not used for the analysis since the M^2AV did not reach the capping inversion due to boundary-layer growth up to $z_i \approx 600$ m in the phase between the mission planning and take-off (see also the discussion in Sect. 4).

Of interest for this study are the radiosonde ascents (light red lines) at 1100 UTC on March 2 and 3. The tethered balloon provided data for March 3 starting at around 0900 UTC (grey box). During all M^2AV flights the variability in z_i, deduced from the remote sensing systems, is substantial. From the available data of the sodar and MCO it is noticeable that during the first flight z_i increased rapidly from approximately 300 m to more than 500 m. During the second flight z_i varied between about 450 and 650 m showing also spatial differences between the two MCO sites. On March 3, 2011 mean z_i increased by about 100 m during both flights.

2.3 Altitude Variability of Flight Legs

The aim of the M^2AV measurements was to characterize the structure of the entrainment zone and to analyze the small-scale turbulent fluctuations in the height range of this zone. Since the vertical range of the entrainment zone is small, flights at constant altitudes with minimum variation were required. The overall six horizontal flight legs of the campaign are used for the analysis; the flight legs are named using their mean altitudes (Fig. 2). The mean altitudes and their standard deviations are presented in Table 1; the standard deviation (σ_z) is below 1.5 m for all flight legs except for leg1_436. With such a good altitude stability it was possible to perform flights within, below and above the entrainment zone, if the exact height range of the entrainment zone was known.

Before take-off a flight schedule was defined. This schedule could have been, in principle, adapted also during the flights, e.g. according to the changing state of the atmosphere. However, this option was not used since the procedure to send atmospheric data to the ground station during flight (and thus e.g. the current temperature profile) was not completed and implemented yet. So at the time of the presented experiment, the state of the atmosphere could not be observed quantitatively on-line during the flight. M^2AV measurements were intentionally combined with remote sensing systems since the actual CBL height was the most important parameter for the planning of the flight. It was estimated from the sodar backscatter data available in real time before each flight. Preparation of the M^2AV for take-off takes about 15 min, so a time delay of up to 20 min occurred between the latest sodar information and take-off. This time delay had to be taken into consideration for the planning

of the altitudes of the flight pattern especially regarding a possible growth of the CBL height. On March 2, the CBL height increased very rapidly during the first flight, which was a problem for the flight planning. The CBL height was underestimated resulting in a too low flight altitude towards the end of the flight.

3 Results

3.1 Detailed Images of the Vertical Structure of the ABL

Monitoring of fast temporal changes of atmospheric conditions in the ABL, especially at the height range of the entrainment zone, is important for analyzing features such as overshooting thermals or downward intrusions of warm and dry air. Thus, on March 2, between 1111 and 1148 UTC (Fig. 4), a flight was performed to gain a detailed image of the vertical structure of the ABL. Additionally the quality of the M^2AV identification of the inversion base was studied.

The flight included four vertical profiles. When flying southward and northward along the path sketched in Fig. 1 the altitude steadily decreased (downward profile) or increased (upward profile), respectively. Each vertical profile consisted of two slant flights, one towards the south and one towards the north (see Fig. 2). The measured potential temperature θ of the first two profiles is presented in Fig. 5; the M^2AV and the radiosonde were equipped with pressure sensors used for the calculation of θ. A good agreement between the UAV

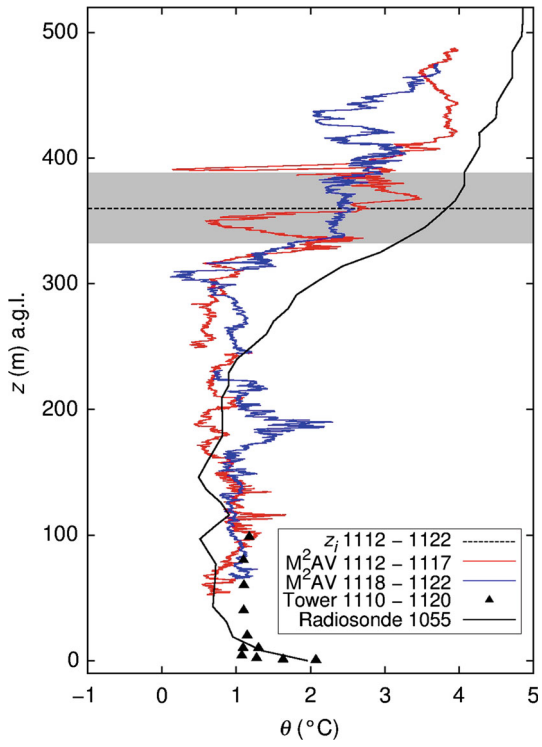

Fig. 5 Vertical profiles on March 2 2011. *Red* (ascent) and *blue* (descent) *lines* present the potential temperature measured by the M^2AV. The *black solid line* shows radiosonde data and the black triangles are the tower data. The CBL height estimated from data of one sodar and two ceilometers during the time of flight and averaged over the three systems is marked with a *horizontal dashed black line* with a *grey area* around it representing the standard deviation of the averaged z_i values. The time periods of the systems are selected to best possibly fit the times of the UAV flight

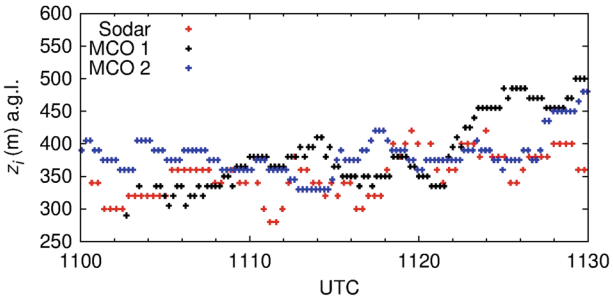

Fig. 6 Convective boundary-layer height estimated from remote sensing systems during the first flight on March 2 2011

(instantaneous profile) and the tower data (averaged over a time period of 10 min) was observed.

The general shape of the radiosonde profile agrees quite well with the M^2AV profile up to about 250 m a.g.l. At that altitude the radiosonde identifies the lower boundary of the temperature inversion (top of the mixed layer, bottom of the inversion layer). In the M^2AV profile this boundary lies at 305 m. The difference can partly be explained by the growth of the CBL during the time of radiosonde ascent and the M^2AV flight. CBL height estimated from the sodar and the ceilometer was found at 360 m ($\pm$ 28 m). Note that the maximum in sodar backscatter and the maximum negative gradient in the ceilometer signal normally occur above the inversion base (Beyrich 1997; Seibert et al. 1998), hence the estimates of z_i from the sodar and the M^2AV are basically consistent. Moreover, as already seen in Fig. 4 during that first flight on March 2, z_i varied considerably in time. For a more detailed analysis Fig. 6 shows the sodar and MCO based z_i values between 1100 and 1130 UTC. Differences in z_i of up to 200 m during these 30 min were observed. The height of the inversion base measured by the UAV ($\approx$305 m) is within the range of variability of the z_i values observed by the remote sensing systems (see Fig. 6).

The fine fluctuations of the potential temperature, which can be seen along the vertical profile of the M^2AV, cannot be resolved by the radiosounding due to its larger sensor inertia combined with its higher ascending speed. The vertical profile of the UAV gives a snap-shot, and the measurement is rather connected to a local limited area than being representative of a larger area. But sharper gradients can be measured and the fine-scale vertical structure of the ABL can be identified. Comparison to remote sensing systems needs to be done carefully because of the different measuring principles and averaging times (see also Martin et al. 2011).

3.2 Detection of Turbulent Bursts

On March 3, 2011 the campaign focused on measurements of turbulent fluctuations and entrainment processes. On that day two flights were performed with three horizontal flight legs each at different altitude levels (Fig. 2; Table 1). During each flight of the campaign two legs were performed in the CBL and one leg was performed within the entrainment zone. Both flights started with a profile sounding up to the highest flight leg, profile segments were flown while descending to the lower flight levels and finally down to $\approx$100 m. The potential temperature measurements during these vertical profiles are presented in Fig. 7, providing information about the atmospheric stratification. Additionally, it can be seen that at the time

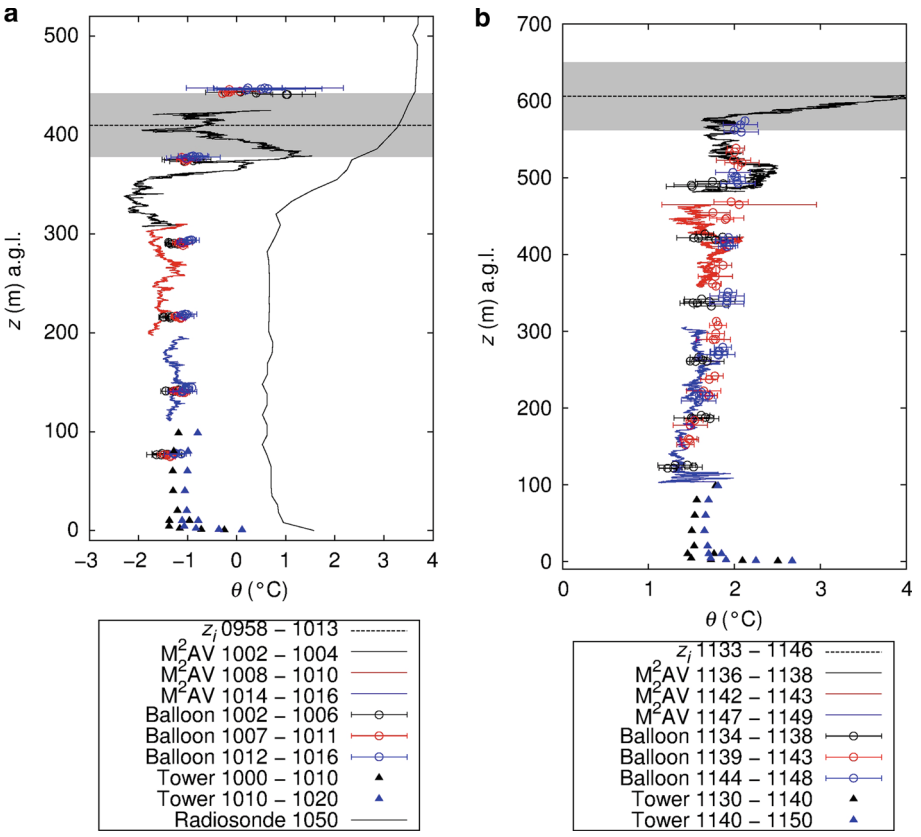

Fig. 7 Vertical profiles on March 3 2011. The *red*, *black* and *blue fluctuating lines* represent the potential temperature measured by the M^{2}AV. The *black solid* and *straight line* shows radiosonde data and the *blue* and *black triangles* are based on tower data. The CBL heights estimated from data of one sodar and two ceilometers during the time of flight and averaged over the three systems is marked with a *horizontal dashed black line* and a *grey box* representing the variability. *Coloured circles* with uncertainties represent measurements of the tethered balloon for different time periods. The time periods of the systems are selected to best possibly fit the times of the UAV flight

of the flights a well-mixed CBL existed. Besides the measurements within the CBL, the flights also included measurements within the temperature inversion layer.

For both profiles M^{2}AV, tower and balloon data agree very well. According to the UAV the bottom of the inversion layer increased from about 350 m a.g.l. during the first flight in the morning to about 580 m a.g.l. during the second flight around noon. The radiosonde temperature data are about 2 K higher than the M^{2}AV, tower and balloon data for the whole profile. The difference can be explained by both the time delay of about 30 min between the radiosonde ascent and the profile flights, and by the spatial separation between the profile soundings. Note that the inversion base in the 1050 UTC radiosonde profile is about 50 m lower than during the first M^{2}AV flight, but this difference is confirmed by the remote sensing systems showing a temporary decrease in z_i at the time of the radiosonde ascent (see Fig. 4). The CBL height estimated by the remote sensing systems is in agreement with the inversion base estimated by the UAV for the second flight. For the first flight z_i values differ by about 50 m. Again, judging this, one should be reminded that the elevated maximum

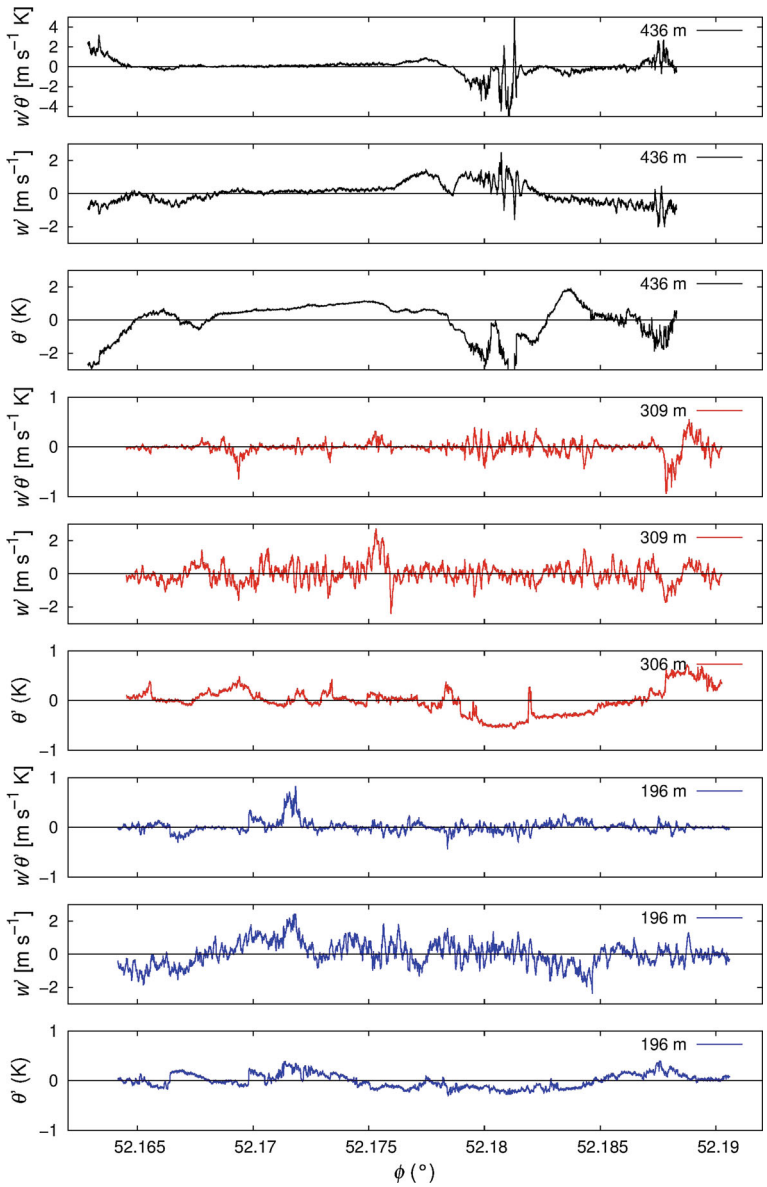

Fig. 8 Spatial series (geographical latitude ϕ) of $w'\theta'$, w' and θ' measured by the M^{2}AV during the first flight on March 3 2011 for the three horizontal flight legs

in sodar backscatter and the maximum negative gradient in the ceilometer signal typically occur above the base of an elevated inversion. Additionally, it needs to be considered that the M^{2}AV provides a local, instantaneous estimate while the remote sensing data have been averaged over the duration of the flight.

For the morning flight, the spatial series of $w'\theta'$, w', and θ' along the flight legs are presented in Fig. 8. The corresponding mean values of $w'\theta'$ are provided in Table 2 as well as the mean vertical velocity variances and the mean potential temperature variances. A strong

Table 2 The mean kinematic sensible heat fluxes $\overline{w'\theta'}$, the vertical velocity variances σ_w^2, and the potential temperature variances σ_θ^2 measured by the M^{2}AV for all legs and one box-flight pattern performed on March 3 2011

Flight number	Leg name	z/z_i	$\overline{w'\theta'}$ (m s^{-1} K)	σ_w^2 (m^2 s^{-2})	σ_θ^2 (K^2)
1	leg1_436	1.07	0.012	0.34	1.63
1	leg1_309	0.75	−0.013	0.32	0.09
1	leg1_196	0.48	0.014	0.49	0.03
2	leg2_625	1.02	−0.223	0.93	0.72
2	leg2_481	0.79	−0.077	0.44	0.19
2	leg2_340	0.56	−0.004	0.48	0.25
2	box2_100	0.17	0.036	0.58	0.26

burst with 340-m horizontal extent at latitude 52.181°N appeared at 436 m above the ground. Such a signal is not found at 309 or 196 m. This event is identified as an overshooting thermal since cold air from below the inversion layer is transported into the inversion layer where on average higher temperatures dominate. Subsequently (at around 52.183°N) warm air was transported downward.

From the spatial series of w' it is also noticeable that there are less turbulent fluctuations of the vertical velocity measured at 436 and 309 m than at the lowest level. The values of the mean vertical velocity variances confirm this observation (see Table 2). Near the top of the CBL the vertical velocity variance is reduced due to stabilization in the free atmosphere overlying the convective mixed layer but also due to the decreasing buoyant energy of the rising thermals (Stull 1988).

The value for the mean potential temperature variance as well as the values of the spatial series of θ' are much larger near $z/z_i \approx 1$ due to entrainment in the presence of large jumps in potential temperature across the CBL top (Lenschow and Wyngaard 1980).

For the second flight the spatial series of $w'\theta'$, w' and θ' are presented in Fig. 9 and the corresponding values for $\overline{w'\theta'}$, σ_w^2, and σ_θ^2 in Table 2. The additional value at ≈100 m in Table 2 comes from a low-level box-flight pattern consisting of four flight legs performed at the end of the second flight on March 3. Presented values for that altitude are averages of the values of the four flight legs. A strong burst is found for $w'\theta'$ at the highest flight level (625 m), which was within the entrainment zone. A second burst is found for $w'\theta'$ at 481 m, which was about 100 m below the entrainment zone. This burst occurred at about the same location as the burst at 625 m height. For this flight the horizontal extent of the burst is about 450 m and it occurs further to the north at latitude 52.182°N, compared to the morning flight. From the spatial series of w' and θ' it is found that at a height of 481 m cold air is transported upwards whereas at 625 m warm air is transported downwards. We hypothesize that this downdraft of warmer air at the boundary-layer top is an entrainment event.

A decrease of $\overline{w'\theta'}$ up to the middle of the entrainment zone ($z/z_i = 1.02$) is found; the values for the mean vertical velocity variance decrease with height as well. The large value for σ_w^2 at $z/z_i = 1.02$ can be explained by the strong burst; the smallest value for σ_θ^2 is measured at $z_i = 0.79$. The additional source of variance due to large jumps in potential temperature across the CBL top lead to the large value for σ_θ^2 at $z_i = 1.02$.

3.3 Vertical Profiles of Normalized Variances

Measurements and numerical studies of the vertical velocity variance σ_w^2 and the potential temperature variance σ_θ^2 can be found in e.g. Deardorff (1974), Lenschow and Wyngaard (1980), Moeng and Wyngaard (1989) and Moene et al. (2006). The results are consistent. During daytime the vertical velocity variance is small near the surface as well as near the

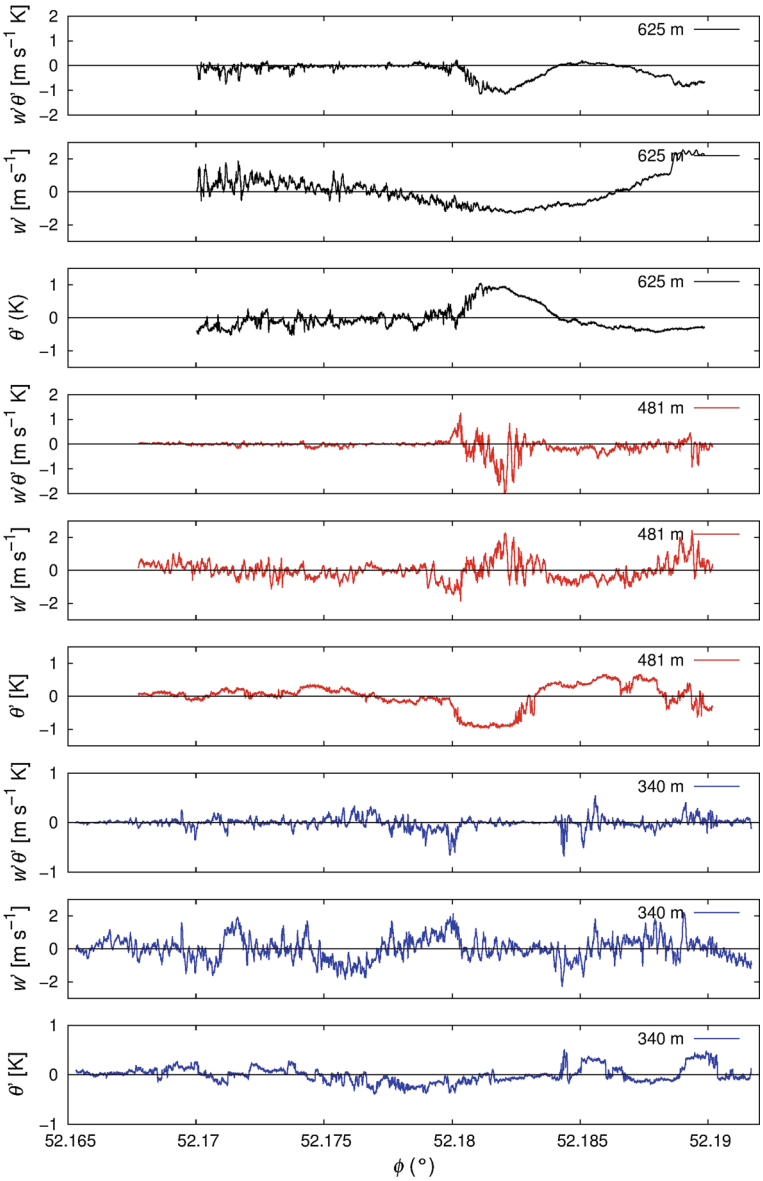

Fig. 9 Spatial series (geographical latitude ϕ) of $w'\theta'$, w' and θ' measured by the M^{2}AV during the second flight on March 3 2011 for the three horizontal flight legs

CBL top; a maximum is found at about a third of z_i. This vertical profile is often described by scaling relations, e.g.,

$$\frac{\sigma_w^2}{w_*^2} = 1.8 \left(\frac{z}{z_i}\right)^{\frac{2}{3}} \left(1 - 0.8\frac{z}{z_i}\right)^2 \tag{1a}$$

with

$$w_* = \left(g z_i \frac{\overline{w'\theta'}_0}{\overline{\theta}} \right)^{\frac{1}{3}} \tag{1b}$$

for the CBL (Lenschow and Wyngaard 1980) with the acceleration due to gravity g, the kinematic sensible heat flux at the ground $\overline{w'\theta'}_0$, and the mean potential temperature in the CBL, $\overline{\theta}$. The development of this vertical structure can be explained by the vertical acceleration of thermals during their initial rise. The vertical velocity variance is reduced near the top of the CBL due to stabilization in the free atmosphere overlying the convective mixed layer but also due to the decreasing buoyant energy of the rising thermals.

During daytime the potential temperature variance is found to be high near the bottom and near the top of the CBL. Close to the surface the magnitude of the variance is increased because of warm thermals being surrounded by a cooler environment. At the height of the inversion the contrast between warmer entrained air and the cooler overshooting thermals can contribute to the variance as well as gravity waves. For the CBL up to $z < 0.4\, z_i$,

$$\frac{\sigma_\theta^2}{\theta_*^2} = 1.8 \left(\frac{z}{z_i} \right)^{-\frac{2}{3}} \tag{2}$$

provides an appropriate description of the profile (Lenschow and Wyngaard 1980). Here the temperature is scaled by its respective free-convection scale

$$\theta_* = \frac{\overline{w'\theta'}_0}{w_*}. \tag{3}$$

Within the framework of this first attempt of using UAV data to analyze entrainment processes it is interesting to see if the UAV data agree with these commonly accepted profile formulations. For the analysis z_i values estimated from the remote sensing systems are taken (see Table 1). The surface flux values, which were needed to calculate w_* and θ_*, were measured by a large aperture scintillometer and by an eddy-covariance measurement system at the field site close to Falkenberg. Since $\overline{w'\theta'}_0$ measured by the LAS and the eddy-covariance station differ, results are presented concerning both systems. For the first flight on March 3, 2011 the LAS measured a surface kinematic sensible heat flux of 0.044 $\mathrm{m\,s^{-1}}$ K and for the second flight 0.049 $\mathrm{m\,s^{-1}}$ K. The eddy-covariance station measured 0.067 $\mathrm{m\,s^{-1}}$ K for the first flight and 0.070 $\mathrm{m\,s^{-1}}$ K for the second flight.

In Fig. 10 the profiles based on the M^{2}AV data are presented. All flight legs introduced in Sect. 2.3 were performed above $z = 0.4\, z_i$. The additional value at ≈100 m in Fig. 10 comes from the low-level box-flight pattern performed at the end of the second flight on March 3, 2011.

Concerning the vertical velocity and the potential temperature variance the UAV data qualitatively confirm the general shape found by previous measurements and numerical studies up to $z/z_i = 1$. Since only a few UAV data are available, this result should be perceived with care. A maximum of the vertical velocity variance at about $z/z_i = 0.3$ is not inconsistent with the data. Above $z = 0.4\, z_i$ the decrease of σ_w with height is found. The influence of the surface heat flux used for scaling is illustrated by the range of the results based on LAS surface heat flux (red crosses) and the results based on the eddy-covariance station (blue circles).

The profile for $\sigma_{\theta.}$ shows a similar pattern to the profile published by Sorbjan (1990) for large-eddy simulation (LES) studies, for which a ratio of entrainment flux to surface flux of $R = -0.4$ was assumed (red line in Fig. 10). At $z/z_i = 0.17$ and $z/z_i = 0.48$ the values for

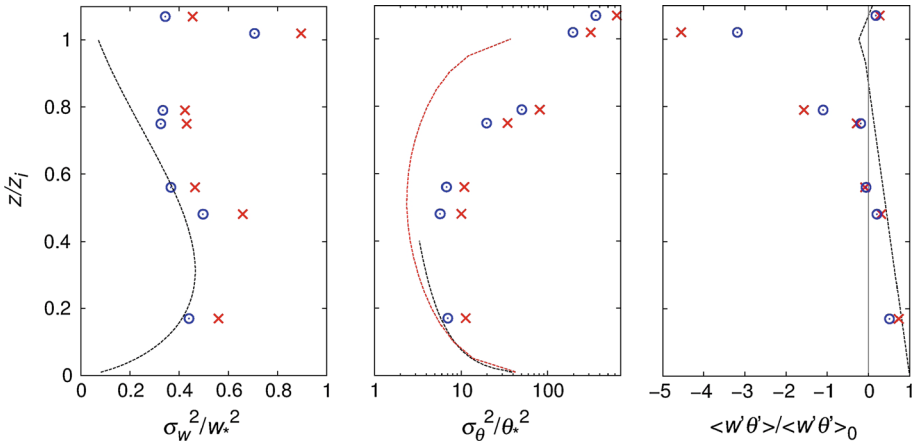

Fig. 10 Vertical profiles of vertical velocity variance (*left*), potential temperature variance (*middle*) and vertical kinematic heat fluxes (*right*) calculated from the M^{2}AV data (the horizontal flight legs on March 3), scaled with the surface heat fluxes measured by the LAS (*red crosses*) and scaled with the surface heat fluxes measured by the eddy-covariance station (*blue circles*). The *lines* represent similarity profiles suggested in the literature: Lenschow and Wyngaard (1980) for σ_w^2 and σ_θ^2 (*black lines*, cf. Eqs. 1a and 2), Moeng and Wyngaard (1989) for the heat flux, and Sorbjan (1990) for σ_θ^2 (*red line*)

$\sigma_\theta^2/\theta_*^2$ are in the order of 10 and increase towards the top of the CBL and the entrainment zone where largest values are found. Again the dependence of $\sigma_\theta^2/\theta_*^2$ on the surface heat flux is noticeable. Besides this dependence, $\sigma_\theta^2/\theta_*^2$ also depends on the ratio of entrainment flux to surface flux as presented by Moeng and Wyngaard (1989) and Sorbjan (1990).

In Fig. 10 (right-hand side) the normalized profile of the measured vertical kinematic sensible heat flux $w'\theta'$ is shown. The dashed line in the diagram represents the buoyancy flux from the LES results published by Moeng and Wyngaard (1989). The values at z/z_i = 1.02 and z/z_i = 0.79 are strongly influenced by the entrainment event and the connected updraft of colder air resulting in large negative fluxes. This clearly indicates, of course, that the second-order statistics (i.e. variances and covariance) calculated by averaging products of turbulent fluctuations measured within the entrainment zone are not significant, i.e. all data points shown in Fig. 10 above approximately $z/z_i = 0.7$ have to be interpreted with great caution, due to the nature of such singular events. However, the downward turbulent flux caused by the entrainment event shows a maximum in the middle of the entrainment zone and vanishes towards $z/z_i = 1.07$. Thus the measured UAV data are in general agreement with the LES simulation.

4 Summary and Conclusions

In this paper first results of using a UAV for the observation of turbulent processes at the top of the CBL are presented. For the first time UAV measurements were performed directly (and intentionally) within the entrainment zone. We are aware of the very limited size of our dataset, consisting of just six horizontal flight legs in the upper part of the convective mixed layer. However, even with this small data base, we find:

(i) The M^{2}AV is able to fly at constant altitude with a typical deviation below 1.3 m, a pre-requisite to study processes inside the often quite thin entrainment zone.

(ii) M^2AV high-resolution wind and temperature measurements allow for very detailed studies of the fine structure of the atmosphere and thus for the identification of quite local and/or short-duration processes such as overshooting thermals or downward intrusions of warm air.
(iii) We could exemplary identify such events in our admittedly small dataset.

It was demonstrated that M^2AV measurements provide highly resolved and detailed images of the vertical structure of the atmosphere at the height range of the capping inversion, which makes the use of this UAV unique. Small-scale processes and sharp gradients are captured by the UAV measurements, which are not detected by the two towers, radiosounding, and the tethered balloon.

In the measured spatial series of the horizontal flight legs the following events were captured:

(i) A strong upward burst of cold air around the top of the boundary layer—an overshooting thermal.
(ii) A strong downdraft of warmer air at the boundary-layer top, which is connected with an updraft of colder air at about $z/z_i = 0.8$—hypothetically an entrainment event.

In the presented data the scaled vertical profiles of vertical velocity, potential temperature variance, and sensible heat flux at least do not disagree with the general shape found by previous measurements and numerical studies. Nevertheless the results have to be valued, judged, and interpreted specifically carefully because of the small amount of data.

These results are reassuring for the potential application of UAV for entrainment studies. Considering atmospheric conditions, it is suggested to perform campaigns in situations with an undisturbed development of the CBL, a maximum inversion base that can safely be reached by the UAV (i.e. within the CAA limitations), and low mixed-layer growth rates such that stationarity can be assumed over short time periods. Experimental entrainment studies with UAV can be simplified by additional use of remote sensing systems, which allow the determination of the height range of the entrainment zone. This information cannot be provided from the instantaneous profile measurements of UAV.

In future campaigns flight mission planning and performance should be improved. For this we see the following approach:

(i) It would be desirable to reduce the flight preparation time from setting the flight pattern to take-off or to make use of the possibility to modify the flight pattern during the flight (adjustment of flight levels) if unexpected z_i values or significant changes in z_i occur during the flight. This requires the in-flight transmission of measured atmospheric data to the ground station, a technology that has become available in the meantime. Nevertheless, we suggest the use of continuous z_i information from sodar or lidar for steering the flight mission, since the UAV itself just provides snapshot-like information that might easily be misinterpreted in the case of, e.g., the UAV crossing an overshooting thermal.
(ii) The representativeness of the pre-flight CBL height information could be improved through spatial information on the boundary-layer structure from, e.g., the operation of a scanning lidar.
(iii) Finally, a simple mixed-layer model, driven by operational on-site data, could be used to improve the nowcasting of the CBL height evolution over the time of the flight.

Acknowledgments We would like to thank C. Behrens and J. Heckmann for their participation in the measurement campaign in Lindenberg in March 2011 and their excellent performance as safety pilots. The

operation of the tethered balloon by R. Begbie and K. Bisek deserves our thanks. We are much obliged to all three anonymous reviewers, their valuable comments contributed to improving the final version. The experiment was funded by the Niedersächsische Technische Hochschule (NTH).

References

Angevine WM, White AB, Avery SK (1994) Boundary layer depth and entrainment zone characterization with a boundary-layer profiler. Boundary-Layer Meteorol 68:375–385

Angevine WM, Grimsdell AW, Hartten LM, Delany AC (1998) The flatland boundary layer experiments. Bull Am Meteorol Soc 79:419–431

Bange J (2009) Airborne measurement of turbulent energy exchange between the Earth surface and the atmosphere. Sierke Verlag, Germany. ISBN 978-3-86844-221-2, 174 pp

Bange J, Spieß T, van den Kroonenberg AC (2007) Characteristics of the early-morning shallow convective boundary layer from Helipod flights during STINHO-2. Theor Appl Climatol 90:113–126

Berger FH, Hantel M (2005) Meteorologisches Observatorium Lindenberg 1905–2005. Meteorol Z 14(5):595

Beyrich F (1997) Mixing height estimation from sodar data—a critical discussion. Atmos Environ 31:3941–3953

Beyrich F, Engelbart DAM (2008) Ten years of operational boundary-layer measurements at the Richard—Aßmann Observatory Lindenberg: the role of remote sensing. IOP Conf Ser Earth Environ Sci 1(012026): 1–6

Beyrich F, Görsdorf U (1995) Composing the diurnal cycle of mixing height from simultaneous sodar and wind profiler measurements. Boundary-Layer Meteorol 76:387–394

Beyrich F, Gryning S-E (1998) Estimation of entrainment zone depth in a shallow convective boundary layer from Sodar data. J Appl Meteorol 37:255–268

Beyrich F, Leps J-P, Mauder M, Foken T, Weisensee U, Bange J, Zittel P, Huneke S, Lohse H, Mengelkamp H-T, Bernhofer C, Queck R, Meijninger WML, Kohsiek W, Lüdi A, Peters G, Münster H (2006) Area-averaged surface fluxes over the heterogeneous LITFASS area from measurements. Boundary-Layer Meteorol 121:33–65

Buschmann M, Bange J, Vörsmann P (2004) MMAV—a miniature unmanned aerial vehicle (Mini-UAV) for meteorological purposes. In: 16th Symposium on boundary layers and turbulence. AMS, Portland/Maine, USA, 9–13 August 2004

Canut G, Lothon M, Saïd F, Lohou F (2010) Observation of entrainment at the interface between monsoon flow and Saharan Air Layer. Q J R Meteorol Soc 136:34–46

Cohn SA, Angevine WM (2000) Boundary layer height and entrainment zone thickness measured by lidars and wind profiling radars. J Appl Meteorol 39:1233–1247

Curry JA, Maslanik J, Holland G, Pinto J (2004) Application of aerosondes in the Arctic. Bull Am Meteorol Soc 85(12):1855–1861

Deardorff JW (1974) Three-dimensional numerical study of turbulence in an entraining mixed layer. Boundary-Layer Meteorol 7:199–226

Deardorff JW, Willis GE, Stockton BH (1980) Laboratory studies of the entrainment zone of a convectively mixed layer. J Fluid Mech 100:41–64

Dias NL, Gonçalves JE, Freire LS, Hasegawa T, Malheiros AL (2012) Obtaining potential virtual temperature profiles, entrainment fluxes, and spectra from mini unmanned aerial vehicle data. Boundary-Layer Meteorol 145:93–111

Emeis S, Münkel C, Vogt S, Müller WJ, Schäfer K (2004) Atmospheric boundary-layer structure from simultaneous sodar, RASS, and ceilometer measurements. Atmos Environ 38:273–286

Holland GJ, Webster PJ, Curry JA, Tyrell G, Gauntlett D, Brett G, Becker J, Hoag R, Vaglienti W (2001) The aerosonde robotic aircraft: a new paradigm for environmental observations. Bull Am Meteorol Soc 82(5):889–901

Lenschow DH, Stankov BB (1986) Length scales in the convective boundary layer. J Atmos Sci 43:1198–1209

Lenschow DH, Wyngaard JC (1980) Mean-field and second-moment budgets in a baroclinic, convective boundary layer. J Atmos Sci 37:1313–1326

Lenschow DH, Mann J, Kristensen L (1994) How long is long enough when measuring fluxes and other turbulence statistics? J Atmos Ocean Technol 11:661–673

Lenschow DH, Krummel PB, Siems ST (1999) Measuring entrainment, divergence, and vorticity on the mesoscale from aircraft. J Atmos Ocean Technol 16:1384–1400

Mann J, Lenschow DH (1994) Errors in airborne flux measurements. J Geophys Res D 99:14519–14526

Martin S, Bange J, Beyrich F (2011) Meteorological profiling of the lower troposphere using the research UAV "M^2AV Carolo". Atmos Meas Tech 4:705–716

Mayer S, Sandvik A, Jonassen MO, Reuder J (2010) Atmospheric profiling with the UAS SUMO: a new perspective for the evaluation of fine-scale atmospheric models. Meteorol Atmos Phys 116(1–2):15–26

Moene AF, Michels BI, Holtslag AAM (2006) Scaling variances of scalars in a convective boundary layer under different entrainment regimes. Boundary-Layer Meteorol 120:257–274

Moeng C, Wyngaard JC (1989) Evaluation of turbulent and dissipation closure in second-order modeling. J Atmos Sci 46:2311–2330

Neisser J, Adam W, Beyrich F, Leiterer U, Steinhagen H (2002) Atmospheric boundary layer monitoring at the Meteorological Observatory Lindenberg as a part of the "Lindenberg Column": Facilities and selected results. Meteorol Z 11:241–253

Nilsson ED, Rannik U, Kulmala M, Buzorius G, O'Dowd CD (2001) Effects of continental boundary layer evolution, convection, turbulence, and entrainment on aerosol formation. Tellus 53B:441–461

Reuder J, Brisset P, Jonassen MO, Müller M, Mayer S (2009) The small unmanned meteorological observer SUMO: a new tool for atmospheric boundary layer research. Meteorol Z 18(2):141–147

Seibert P, F Beyrich, SE Gryning, S Joffre, A Rasmussen, P Tercier (1998) Mixing height determination for dispersion modeling. In: Fisher BEA et al (eds) Harmonization of the pre-processing of meteorological data for atmospheric dispersion models COST action 710—final report. European Commission Publication No. EUR 18195 EN (ISSN 1018–5593), Brussels, 120 pp

Siebert H, Wendisch M, Conrath T, Teichmann U, Heintzenberg J (2003) A new tethered balloon-borne payload for fine-scale observations in the cloudy boundary layer. Boundary-Layer Meteorol 106:461–482

Sorbjan Z (1990) Similarity scales and universal profiles of statistical moments in the convective boundary layer. J Appl Meteorol 29(8):762–775

Spieß T, Bange J, Buschmann M, Vörsmann P (2007) First application of the meteorological Mini-UAV "M^2AV". Meteorol Z 16:159–169

Stull RB (1988) An introduction to boundary layer meteorology. Kluwer, Dordrecht, 666 pp

Stull RB (2000) Meteorology for scientists and engineers, 2nd edn. Brooks/Cole Division, Thompson Learning Company, 502 pp

Träumner K, Kottmeier C, Corsmeier U, Wieser A (2011) Convective boundary-layer entrainment: short review and progress using Doppler lidar. Boundary-Layer Meteorol 141:369–391

van den Kroonenberg AC, Martin T, Buschmann M, Bange J, Vörsmann P (2008) Measuring the wind vector using the autonomous mini aerial vehicle M^2AV. J Atmos Ocean Technol 25:1969–1982

van den Kroonenberg AC, Martin S, Beyrich F, Bange J (2011) Spatially-averaged temperature structure parameter over a heterogeneous surface measured by an unmanned aerial vehicle. Boundary-Layer Meteorol 142:55–77